Supporting Information:

Bubble-Mediated Formation of Airborne Nanoplastic Particles

Eva R. Kjærgaard[1], *Freja Hasager*[1], *Sarah S. Petters*[1,2], *Marianne Glasius*[1], *Merete Bilde*[1*]

[1]Department of Chemistry, Aarhus University, DK-8000 Aarhus C, Denmark

[2] Current address: Center for Environmental Research and Technology, University of California, Riverside, 92507 California, USA

This supplement contains 21 pages.

*Corresponding: **Merete Bilde** – Department of Chemistry, Aarhus University, DK-8000 Aarhus, Denmark. orcid.org/0000-0002-2112-514X, bilde@chem.au.dk. Authors: **Eva R. Kjærgaard** – orcid.org/0000-0001-8838-0084. **Freja Hasager** – orcid.org/0000-0002-1256-1468. **Sarah S. Petters** – orcid.org/0000-0002-4501-7127. **Marianne Glasius** – orcid.org/0000-0002-4404-6989.

Table of Contents

SECTION S1: EXPERIMENTAL SUPPLEMENT

S1.1 Synthetic sea salt

Table S1. Information on the synthetic sea salt used in this study, which was mixed following Nielsen and Bilde [1].

Salt	M_w (g mol^{-1})	Purity *	CAS Number
NaCl	58.44	Puriss, p.a. ≥ 99.5 % (AT)	7647-14-5
$MgCl_2 \cdot 6H_2O$	203.30	BioXtra ≥ 99.0 %	7791-18-6
$CaCl_2 \cdot 2H_2O$	147.01	BioUltra for molecular biology ≥ 99.5 % (RT)	10035-04-8
KNO_3	101.10	BioUltra for molecular biology ≥ 99.5 % (RT)	7757-79-1
NaBr	102.89	≥ 99.0 % ACS reagent	7647-15-6
K_2SO_4	174.26	≥ 99.0 % ACS reagent	7778-80-5
Na_2SO_4	142.04	≥ 99.0 % ACS reagent	7757-82-6

* Supplier: Sigma-Aldrich

S1.2 Schematic of the experimental set-up

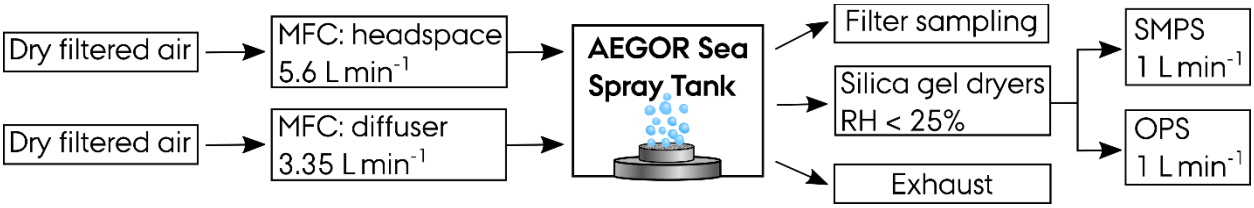

Figure S1. Schematic of the experimental set-up and flows, used in this study. See also Christiansen et al. 2019.[2] In Experiment 5 a consecutive series of experiments were performed with an HTDMA and an aerosol mass spectrometer attached to the headspace, these are further described in Petters et al.[3] Filter sampling was performed in some experiments (2, 4 and 5d) after completion of the SMPS measurements. During filter sampling the SMPS and OPS were not running.

S1.3 AEGOR headspace equilibrium considerations

S1.3.1 Flow diagram

Figure S2 is a simplified flow diagram of the AEGOR headspace. In the tank headspace, the incoming clean air (flow Q_{in}, L/min) carries no particles. The outgoing air carries particles with time-dependent concentration $c(t)$, or $\frac{1}{V}N(t)$. An additional source of particles is the bubbling, which provides a constant $\frac{dN}{dt}_{bubble}$ of r_0 in units of # L^{-1} min^{-1}.

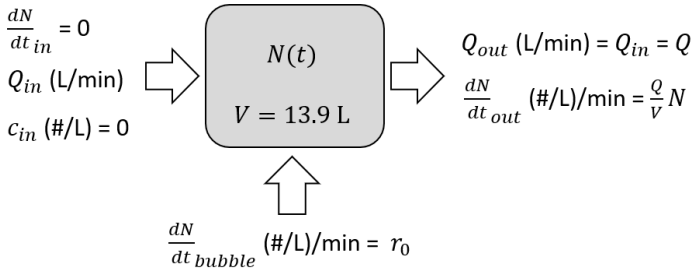

Figure S2. Diagram for time-dependent concentration of particles in the tank. The total flow in, Q, is 8.95 L min^{-1}, and the flow out is split between waste and instruments.

The equation describing the change in number concentration in the tank is therefore:

$$\frac{dN(t)}{dt} = -\frac{dN}{dt}_{out} + \frac{dN}{dt}_{bubble} + \frac{dN}{dt}_{in} \quad \text{(S1)}$$

$$\frac{dN(t)}{dt} = -\frac{dN}{dt}_{out} + r_0 + 0 \quad \text{(S2)}$$

$$\frac{dN(t)}{dt} = r_0 - \frac{dN}{dt}_{out} \quad \text{(S3)}$$

Equation S3 can be solved for $N(t)$ by using the integrating factor method. The equation can be expressed in a standard form $\frac{dy}{dx} + a(x)y = b(x)$ with a solution $y(x) = \exp^{-1}(\int a(x)dx)\,(B(x) + C_3)$, where C_3 is an integration constant and the term $B(x)$ is defined by $B(x) = \int\left(\ e^{\int a(x)dx}\ b(x)\ \right)dx$. The integrating factor is $e^{\int a(x)dx}$ and is defined to assist in the derivation.

Section S1.3.2 The solution

A series of steps are taken to match the equation set up for AEGOR with the solution in its standard form:

Standard form	This work	
$\frac{dy}{dx} + a(x)y = b(x)$	$\frac{dN(t)}{dt} + \frac{Q}{V}N(t) = r_0$	(S4)
x	t	(S5)
y	$N = N(t)$	(S6)
$a(x)$	$Q/V = constant$	(S7)
$b(x)$	$r_0 = constant$	(S8)
$\int a(x)dx$	$\int \frac{Q}{V} dt = \frac{Qt}{V}$	(S9)
Integration factor: $e^{\int a(x)dx}$	$e^{Qt/V}$	(S10)
$b(x)e^{\int a(x)dx}$	$r_0 e^{Qt/V}$	(S11)
$B(x) = \int \left(b(x)e^{\int a(x)dx}\right)dx$	$B(x) = \int \left(r_0 e^{Qt/V}\right) dt = \frac{r_0 V}{Q} e^{Qt/V}$	(S12)
$B(x) + C_3$	$\frac{r_0 V}{Q} e^{Qt/V} + C_3$	(S13)
$y = e^{-\int a(x)dx}(B(x) + C_3)$	$N(t) = e^{-Qt/V}\left(\frac{r_0 Q}{V} e^{Qt/V} + C_3\right)$	(S14)
$y = C_3\, e^{-\int a(x)dx} + B(x)\, e^{-\int a(x)dx}$	$N(t) = C_3 e^{-Qt/V} + r_0 Q/V$	(S15)

Solution

The initial value problem is solved to find C_3:

$$N(t=0) = 0 \quad \text{(S16)}$$

$$C_3 e^0 + \frac{r_0 Q}{V} = 0 \quad \text{(S17)}$$

$$C_3 = -\frac{r_0 Q}{V} \quad \text{(S18)}$$

The general form of the solution is:

$$N(t) = \frac{r_0 Q}{V}\left(1 - e^{-Qt/V}\right) \quad \text{(S19)}$$

Equilibrium concentration

To find the equilibrium concentration, the solution is assessed at $t = \infty$.

$$N(t=\infty) = \frac{r_0 Q}{V}\left(1 - e^{-Q\infty/V}\right) \quad \text{(S20)}$$

$$N(t=\infty) = \frac{r_0 Q}{V} \quad \text{(S21)}$$

The equilibrium concentration is $r_o Q/V$.

Equilibrium time

The time to reach 95% of the equilibrium concentration, τ_{95}, is found as follows:

$$0.95\frac{r_0 Q}{V} = \frac{r_0 Q}{V}\left(1 - e^{-Q\tau_{95}/V}\right) \quad \text{(S22)}$$

$$0.95 = 1 - e^{-Q\tau_{95}/V} \quad \text{(S23)}$$

$$e^{-Q\tau_{95}/V} = 1 - 0.95 \quad \text{(S24)}$$

$$-\frac{Q\tau_{95}}{V} = \ln(0.05) \quad \text{(S25)}$$

$$\tau_{95} = -\frac{\mathrm{V}}{\mathrm{Q}}\ln(0.05) \quad \text{(S26)}$$

The volume of the headspace, V, is 13.9 L, and total flow, Q, is 5.6 + 3.35 = 8.95 L min^{-1}. The time to reach 95% of equilibrium is:

$$\tau_{95} = -\frac{13.9\ \mathrm{L}}{8.95\ \mathrm{L/min}}\ln(0.05) = -\frac{13.9}{8.95}(-2.9957)\ \mathrm{min} = 4.6526\ \mathrm{min}$$

which is about 280 s or 4.7 minutes.

SECTION S2. INTEGRATION OF SMPS NUMBER DISTRIBUTIONS

The PSL number concentrations, presented in Table 2 in the manuscript, were determined by fitting a single log-normal distribution to dN/dlog(Dp) versus Dp (see Table S2 for fitting parameters).. For Experiment 5, which contained salt, the PSL number concentration was also determined by a sum of 2 log-normal distributions (equation 8.54 in Seinfeld and Pandis[4]):

$$n_N(\log Dp) = \sum_{i=1}^{n} \frac{N_i}{(2\pi)^{\frac{1}{2}} \log \sigma_i} \exp\left(-\frac{(log\, Dp - log\, \bar{D}p_i)^2}{2log^2\sigma_i}\right) \quad \text{(S27)}$$

where N_i is the number concentration, $\bar{D}p_i$ is the median particle diameter and σ_i is the standard deviation of the i'th lognormal mode. The obtained fitting parameters for the double log-normal fits are given in Table S3. Due to the very large difference in number concentration of salt and PSL particles, fitting a sum of log-normal distributions to the data is challenging. Therefore, the single log-normal distribution fits to this data can be considered as upper-limit number concentration values. For single log-normal fits it was not possible to fit experiment 5e due to large influence of salt and experiment 6a and 6b due to low signal. Regarding Table 2 number concentration values reported in the main manuscript, for experiment 5e the double log-normal fit value was used and for experiments 6a and 6b the sum of dN values over the range of 60-155 nm was used.

Table S2. Fitting parameters for a single log-normal fit of dN/dlog(Dp) as a function of Dp. N_1 is the number concentration, Dp_1 is the median diameter and σ_1 is the standard deviation. It was not possible to fit Experiment 5e and 6a-6b.

Experiment	N_1 (cm^{-3})	σ_1	Dp_1 (nm)	Fitting range (nm)
1	12.54	1.071	145.0	70.4-355.5
2	29.74	1.070	145.0	70.4-355.5
3a	12.73	1.070	145.0	70.4-355.5

3b	5.591	1.071	144.3	70.4-355.5
3c	2.119	1.083	144.2	70.4-355.5
3d	1.420	1.154	145.4	100.9-207.2
4	3.039	1.083	262.1	70.4-537.6
5 *	10.45	1.071	142.6	70.4-537.6
5a	30.10	1.095	142.6	70.4-537.6
5b	24.14	1.078	143.2	70.4-355.5
5c	25.15	1.084	143.8	100.9-355.5
5d	33.78	1.102	142.9	118.64-355.5
5e	-	-	-	-
6a	-	-	-	-
6b	-	-	-	-
6c	31.42	1.167	97.77	59.89-155.38
6d	44.76	1.150	98.39	59.89-155.38
6e	56.81	1.161	98.04	59.89-155.38
6f	71.99	1.155	98.10	59.89-155.38

*Data have been baseline corrected. Without baseline correction $N_1 = 18$ cm^{-3}.

Table S3. Fitting parameters for a sum of 2 log-normal fits of dN/dlog(Dp) as a function of Dp for salinity experiments ranging from 0.01 to 0.2 g kg^{-1} (Experiment 5). N_i is the number concentration, Dp_i is the median diameter and σ_i is the standard deviation of the i'th lognormal mode. The PSL peak is mode 2.

	N_1 (cm^{-3})	σ_1	Dp_1 (nm)	N_2 (cm^{-3})	σ_2	Dp_2 (nm)	Fitting range (nm)
5a: 0.01 g kg^{-1}	333.8	1.883	29.19	24.6	1.0771	143.6	58.8-355.5
5b: 0.02 g kg^{-1}	314.7	1.669	31.58	22.6	1.0730	143.6	74.3-355.5
5c: 0.05 g kg^{-1}	294.6	1.410	23.20	23.2	1.0765	144.4	85.8-355.5
5d: 0.1 g kg^{-1}	1875	1.307	55.01	28.6	1.0838	144.9	84.3-355.5
5e: 0.2 g kg^{-1}	3379	1.299	66.55	40.7	1.1026	147.1	100.9-355.5

SECTION S3. FILTER SAMPLING

Aerosol filters from Experiments 2, 4 and 5d, were analyzed with py-GC-MS by preparing filter punch outs of 3 mm diameters, which were analyzed in triplicates.

Sampling on filters was performed overnight: Experiment 2: 14 hrs 17 min, 2.9 L min^{-1} flowrate), Experiment 4: 20 hrs 33 min, 1.6 L min^{-1} flow rate and Experiment 5d: for salinity 0.1 g/kg 14 hrs 9 min, 1.6 L min^{-1} flow rate.

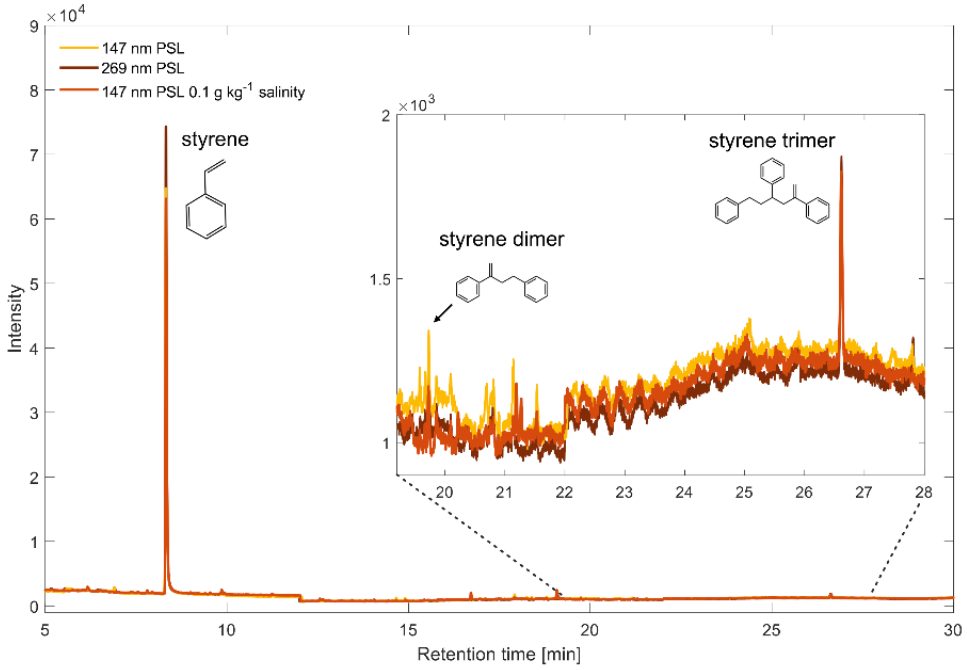

Figure S4. Pyrograms from the py-GCMS analysis of particle filters collected during the experiments with 147 nm PSL in milli-Q water (yellow), 269 nm PSL in milli-Q water (brown), and 147 nm PSL in 0.1 g kg^{-1} saline water (orange). The inset shows a zoom of the 19-28 min retention time window. Peaks from polystyrene marker compounds are labeled.

Figure S4 shows the pyrograms obtained from py-GCMS analysis of filter punch-outs from experiments 2, 4, and 5d. During pyrolysis, polystyrene fragments into the styrene monomer,

styrene dimer, and styrene trimer. The styrene monomer can arise from the pyrolysis of several synthetic polymers, while the styrene dimer and trimer are characteristic only of polystyrene. The presence of these two marker compounds confirms that polystyrene particles were collected on the filters in the three experiments.

SECTION S4. EXPERIMENTAL TIME EVOLUTION OF PSL NUMBER CONCENTRATION

Figures S5a – S5d show the number concentration of polystyrene (PSL) particles as a function of experiment time, obtained by taking a sum of the number concentration (dN) in the range of the PSL peak in the SMPS spectra. The range was chosen from the log-normal fit to the PSL peak, where the number concentration value was smaller than 0.1 cm^{-3}.

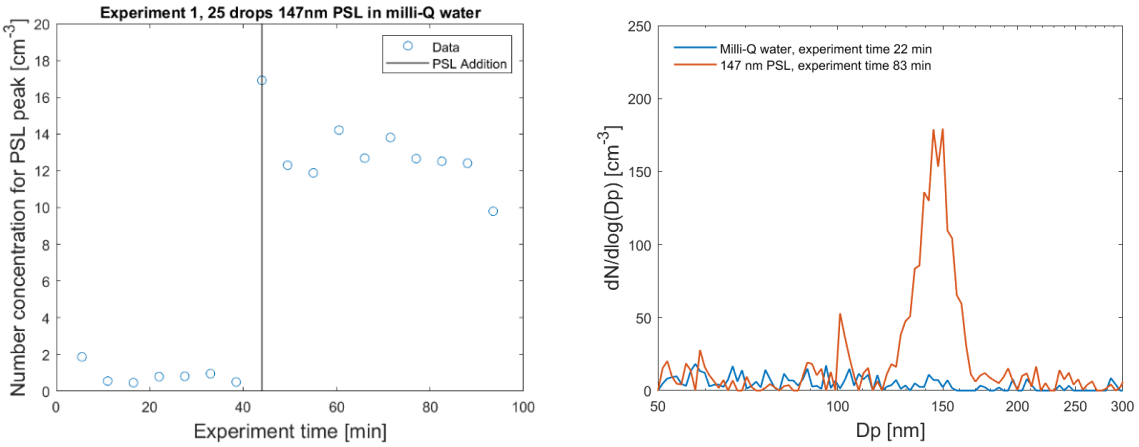

Figure S5a. Number concentration of PSL particles as a function of experimental time for experiment 1 (blue). The black line shows the time at which the tank was opened and PSL was added. The number concentration was obtained by taking a sum of dN values in the range 110-189 nm, corresponding to the PSL peak. The left figure shows a comparison of a scan of milli-Q water and after PSL addition.

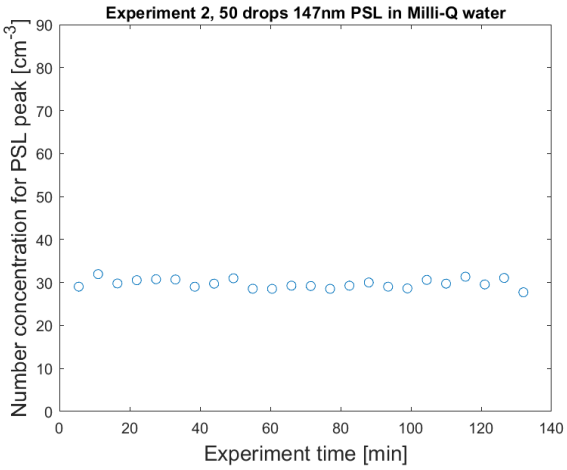

Figure S5b. Number concentration of PSL particles as a function of experimental time for experiment 2. The number concentration was obtained by taking a sum of dN values in the range 110-189 nm, corresponding to the PSL peak. The left figure shows a comparison of a scan of milli-Q water and after PSL addition.

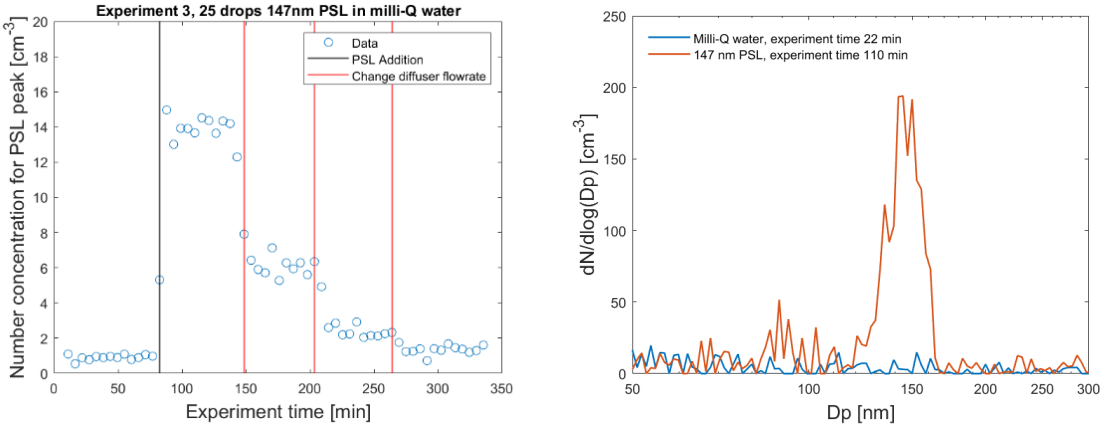

Figure S5c. Number concentration of PSL particles as a function of experimental time for experiment 3 (blue). The black line shows the time at which the tank was opened and PSL was added. The red lines show the time when the diffuser flow rate was decreased. The number concentration was obtained by taking a sum of dN values in the range 110-189 nm, corresponding to the PSL peak. The left figure shows a comparison of a scan of milli-Q water and after PSL addition.

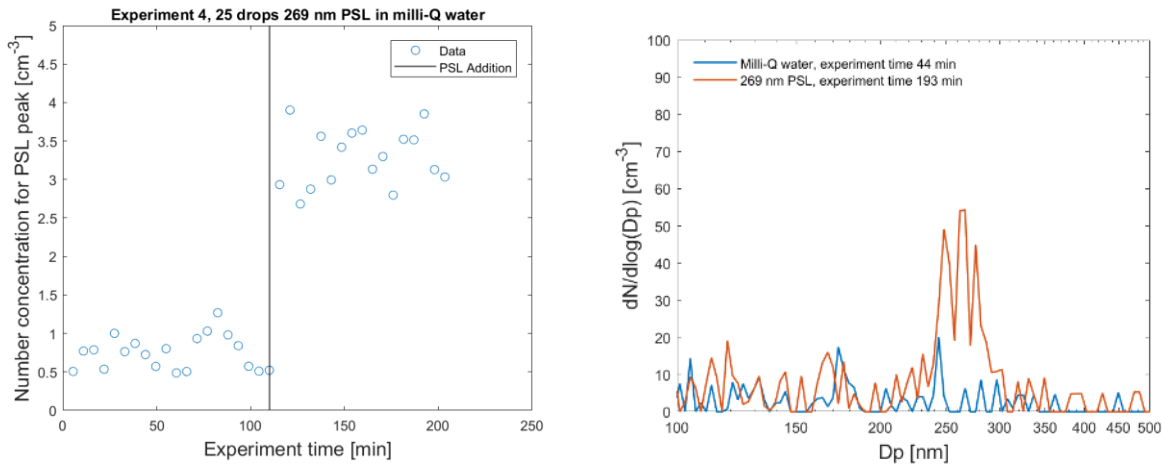

170

171 **Figure S5d.** Number concentration of PSL particles as a function of experimental time for experiment 4 (blue). The
172 black line shows the time at which the tank was opened and PSL was added. The number concentration was obtained
173 by taking a sum of dN values in the range 196-350 nm, corresponding to the PSL peak. The left figure shows a
174 comparison of a scan of milli-Q water and after PSL addition.

175

176

SECTION S5. SMPS TRANSFER FUNCTION

Figure S6 shows a comparison of the experimental results for 25 drops of 147 nm PSL in milli-Q water (orange) from Experiment 1, and the SMPS transfer functions. The purple function is the probability density functional (PDF) centered at 147 nm for the 4.3 nm standard deviation that is given for the diameter of the PSL nanospheres. The experimental results show a peak wider than the standard deviation of the PSL nanospheres (orange vs. purple) and therefore the width of the peak cannot arise solely from this. The black lines in Figure S6 represent the outer lines of a non-diffuse transfer function for a flow ratio of β=1.0/5.0 (δ=0) at DMA centroid diameter D_p^* = 147 nm, calculated with Stolzenburg and McMurry[5]. These bounds are slightly wider than the experimental results shown in orange, which means the widening of the experimental PSL peak can be explained by the transfer function.

Additionally, we have calculated the overlap (green function in Figure S6) of the theoretical transfer functions for each bin with the PDF of the PSL nanospheres. This was done by calculating a non-diffuse transfer function for a flow ratio of β=1.0/5.0 (δ=0) and DMA centroid diameters ranging D_p^* = 10-300 nm in intervals of 1 nm. Then creating a probability density functional for each. By multiplying the calculated PDFs with the PDF for the PSL nanospheres (the purple function in Figure S6) we obtain the overlap for each point in the diameter range. These are summed giving a value for the overlap between the transfer functions for each bin with the PDF of the PSL nanospheres, plotted in green in Figure S6. This function is slightly wider than the experimental PSL peak, which again shows that the widening of the experimental PSL peak can be explained by the transfer function.

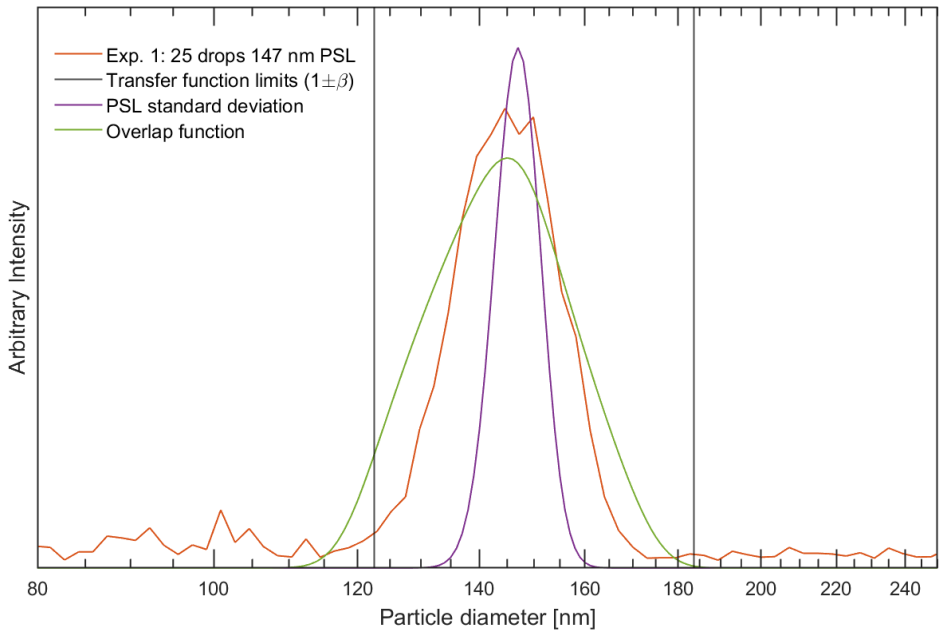

Figure S6. Experimental results for 25 drops of 147 nm PSL in milli-Q water (orange) from Experiment 1. The black lines represent the outer lines of a non-diffuse transfer function for a flow ratio of β=1.0/5.0 (δ=0) at DMA centroid diameter D_p^* = 147 nm, calculated with Stolzenburg and McMurry[5]. The purple function is the probability density functional (PDF) centered at 147 nm for the 4.3 nm standard deviation that is given for the diameter of the PSL nanospheres (multiplied by a factor 2000 to obtain comparable y-axis). The green function shows the overlap of the transfer function for each bin with the PDF of the PSL nanospheres, the purple function, multiplied by a factor 5000 to obtain comparable y-axis.

SECTION S6. FULL SMPS SIZE SPECTRA

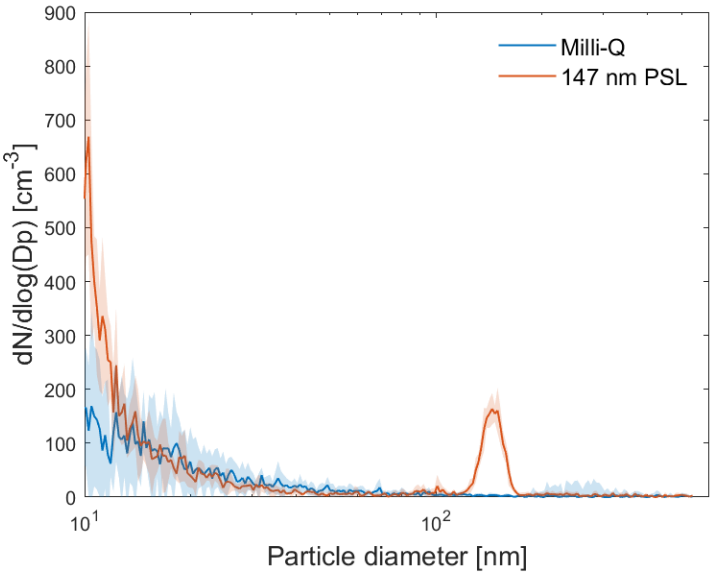

Figure S7a. Mean particle number size distribution measured by the SMPS (headspace air) for a solution of 20 L milli-Q water (blue) and after addition of 25 drops of 147 nm PSL (orange), from Experiment 1. Diffuser flow rate of 3.35 L min^{-1} and temperature was held constant at 20°C. All data are averaged of 30 min (5 scans) and 1 standard deviation is shown as a shading.

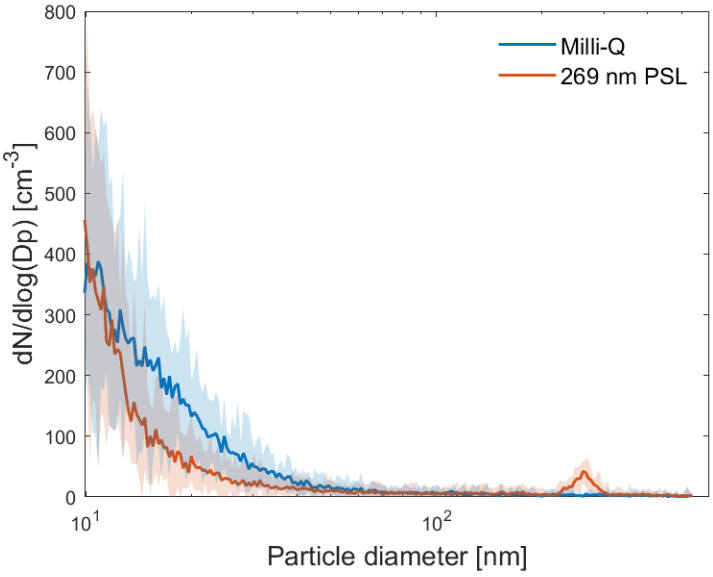

Figure S7b. Mean particle number size distribution measured by the SMPS (headspace air) for a solution of 20 L milli-Q water (blue) and after addition of 25 drops of 269 nm PSL (orange) from Experiment 4. Diffuser flow rate of 3.35 L min^{-1} and temperature was held constant at 20°C. All data are averaged of 30 min (5 scans) and 1 standard deviation is shown as a shading.

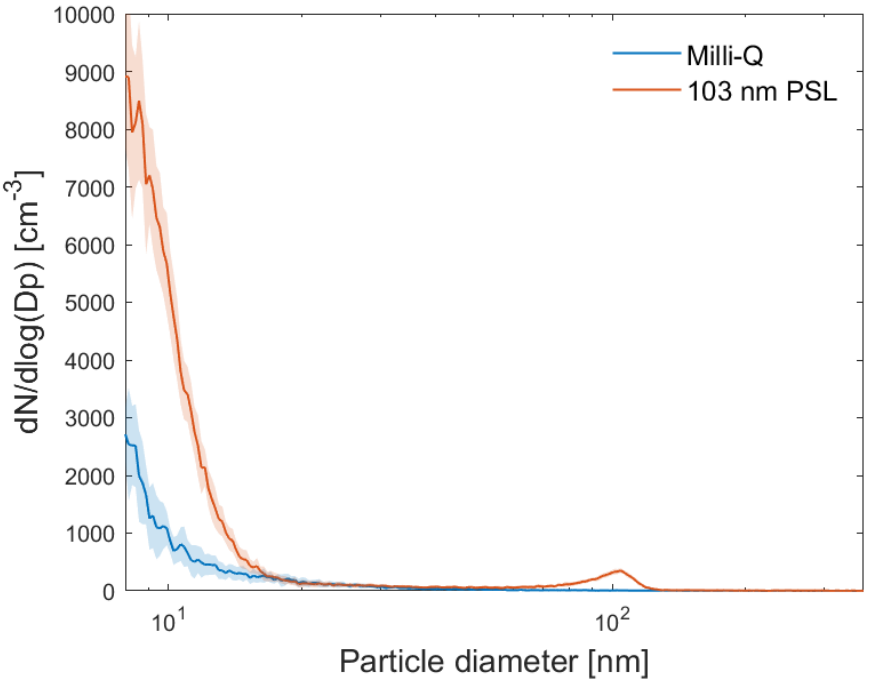

Figure S7c. Mean particle number size distribution measured by the SMPS (headspace air) for a solution of 20 L milli-Q water (blue) and after addition of 30 drops of 103 nm PSL (orange) from experiment 6. Diffuser flow rate of 3.35 L min^{-1} and temperature was held constant at 20ºC. All data are averaged of 30 min (5 scans) and 1 standard deviation is shown as a shading.

SECTION S7. PARTICLES OUTSIDE THE PSL PEAKS

The optical spectrum reported by the OPS in the size range 0.3–10 µm showed fewer than 1 particle cm^{-3} (Figure S8; Experiment 1 in Table 1). The mobility spectra reported by the SMPS data ranging from the PSL peak up to 538 nm showed no clear peaks above the signal-to-noise limit. In Experiment 1, fewer than 8 cm^{-3} particles are observed above 200 nm, and in Experiment 4 fewer than 1 cm^{-3} particles are observed above 300 nm (see Section S6).

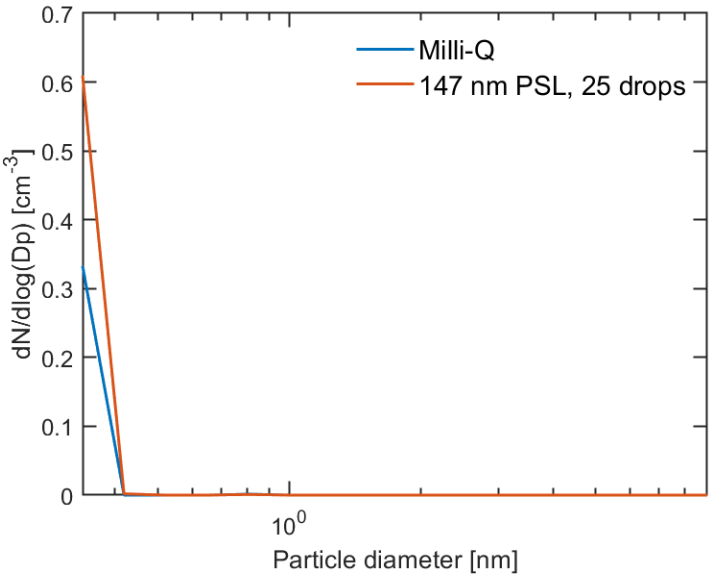

Figure S8. Mean particle number size distribution measured by the OPS for a solution of 20 L milli-Q water (blue) and after addition of 25 drops of 147 nm PSL (orange) from experiment 1. Diffuser flow rate of 3.35 L min^{-1} and a constant temperature of 20°C. Data are averaged over 15 min for Milli-Q and 55 min for PSL. Note the y-axis goes from 0-0.7 cm^{-3}.

SECTION S8. TEST OF REPRODUCIBILITY

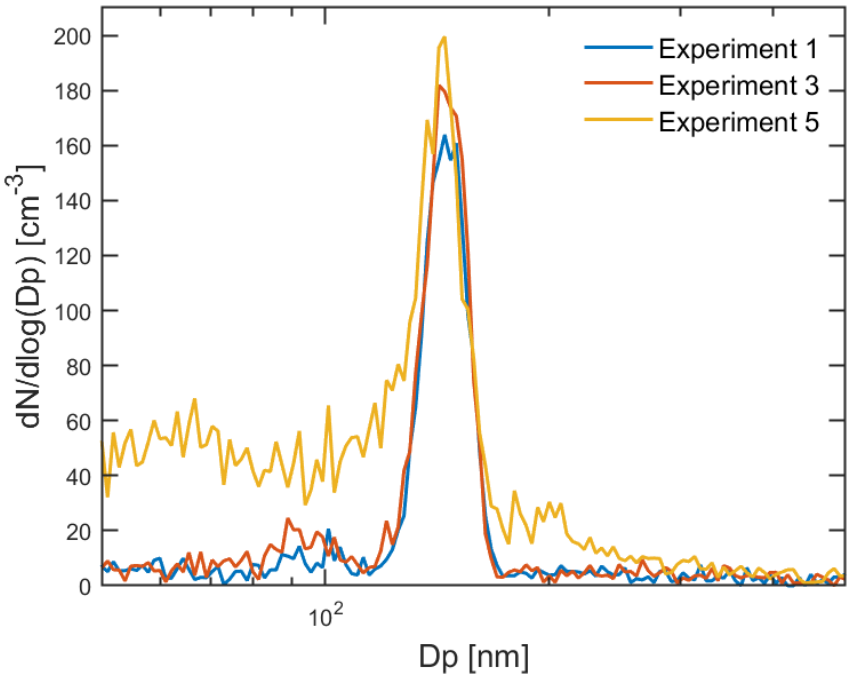

Figure S9. Mean particle number concentration measured from the headspace in AEGOR by the SMPS for a solution of 20 L milli-Q water containing 25 drops of 147 nm PSL. Experiments were performed with the diffuser set to 3.35 L min^{-1} and a constant temperature of 20°C. Comparison of Experiment 1 (blue), Experiment 3 (orange) and Experiment 5 (yellow, 0 g kg^{-1} salt). All data is an average of 30 min (5 scans) measurement.

The particle number size distributions from the three experiments show the same shape and the integrated number concentrations of the PSL peak differ by less than three particles cm^{-3}: Experiment 1 (12.5 cm^{-3}) and Experiment 3 (12.7 cm^{-3}) based on log-normal fitting, Experiment 5 (0 g kg^{-1} salt) the number concentration is 10.5 cm^{-3} accounting for the background (see also S31).

SECTION S9. SALT EXPERIMENTS

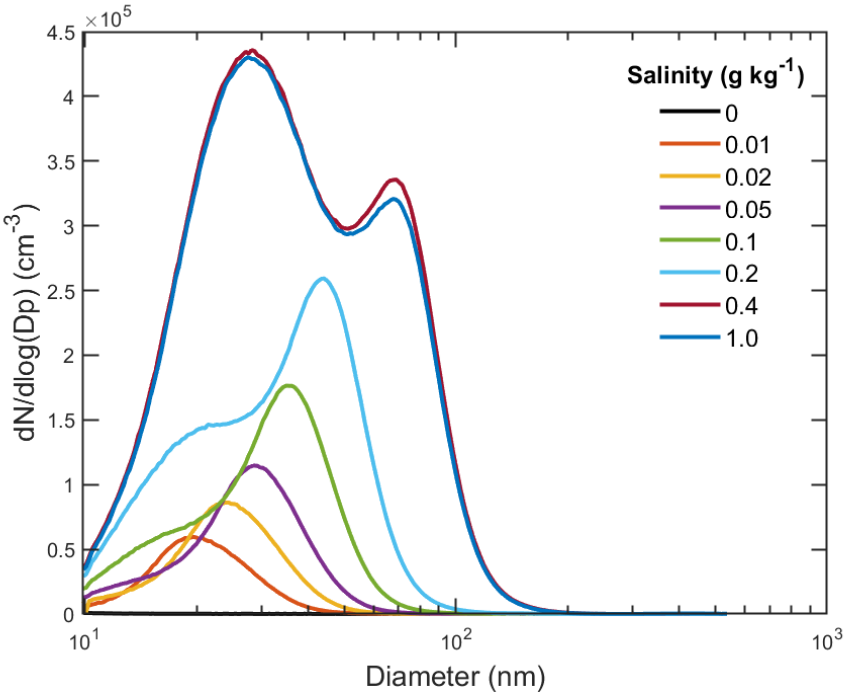

Figure S10. Mean particle number size distribution measured by the SMPS for a solution of 20 L milli-Q water containing 25 drops of 147 nm PSL and varying salinity of sea salt. Diffuser set to 3.35 L min^{-1} and a constant temperature of 20 °C (Experiment 5). All data is an average of 78 min (13 scans).

REFERENCES

1. Nielsen, L. S.; Bilde, M., Exploring Controlling Factors for Sea Spray Aerosol Production: Temperature, Inorganic Ions and Organic Surfactants. *Tellus B: Chemical and Physical Meteorology* **2020**, *72*, 1-10.
2. Christiansen, S.; Salter, M. E.; Gorokhova, E.; Nguyen, Q. T.; Bilde, M., Sea Spray Aerosol Formation: Laboratory Results on the Role of Air Entrainment, Water Temperature, and Phytoplankton Biomass. *Environmental Science & Technology* **2019**, *53*, 13107-13116.
3. Petters, S. S.; Kjærgaard, E. R.; Hasager, F.; Massling, A.; Glasius, M.; Bilde, M., Morphology and Hygroscopicity of Nanoplastics in Sea Spray. *Physical Chemistry Chemical Physics* **2023**.
4. Seinfeld, J. H.; Pandis, S. N., *Atmospheric Chemistry and Physics: From Air Pollution to Climate Change*; John Wiley & Sons, 2016.
5. Stolzenburg, M. R.; McMurry, P. H., Equations Governing Single and Tandem Dma Configurations and a New Lognormal Approximation to the Transfer Function. *Aerosol Science and Technology* **2008**, *42*, 421-432.